

Inorganic salts of biguanide – Searching for new materials for second harmonic generation

Irena Matulková^{a,*}, Ivan Němec^a, Ivana Císařová^a, Petr Němec^b, Zdeněk Mička^a

^a Charles University in Prague, Faculty of Science, Department of Inorganic Chemistry, Hlavova 2030, 128 40 Prague 2, Czech Republic

^b Charles University in Prague, Faculty of Mathematics and Physics, Department of Chemical Physics and Optics, Ke Karlovu 3, 121 16 Prague 2, Czech Republic

Received 5 October 2007; received in revised form 31 October 2007; accepted 4 November 2007

Available online 21 November 2007

Abstract

Five inorganic salts of biguanide with carbonic, nitric, phosphoric and phosphorous acids were prepared and X-ray structural analysis has been performed for three novel compounds. Biguanidium(1+) phosphite trihydrate crystallizes in the triclinic space group $P\bar{1}$, $a = 7.1470(1) \text{ \AA}$, $b = 9.6530(2) \text{ \AA}$, $c = 11.3140(2) \text{ \AA}$, $\alpha = 70.094(1)^\circ$, $\beta = 75.688(1)^\circ$, $\gamma = 86.099(1)^\circ$, $V = 713.71(2) \text{ \AA}^3$, $Z = 2$, $R = 0.0350$ for 3031 observed reflections. The crystal structure is based on a network of phosphite anions and water molecules. Biguanidium(1+) cations form pairs through two intermolecular hydrogen bonds of the N–H...N type and fill the network with anions and water molecules.

Biguanidium(2+) phosphite monohydrate crystallizes in the triclinic space group $P\bar{1}$, $a = 6.9690(2) \text{ \AA}$, $b = 7.3500(3) \text{ \AA}$, $c = 8.1730(3) \text{ \AA}$, $\alpha = 82.518(2)^\circ$, $\beta = 83.015(2)^\circ$, $\gamma = 82.811(2)^\circ$, $V = 409.44(3) \text{ \AA}^3$, $Z = 2$, $R = 0.0308$ for 1779 observed reflections. The structure is formed of a network of alternating biguanidium(2+) cations, phosphite anions and pairs of water molecules interconnected by a system of intermolecular hydrogen bonds.

Biguanidium(2+) hydrogen phosphate monohydrate crystallizes in the triclinic space group $P\bar{1}$, $a = 7.0630(2) \text{ \AA}$, $b = 7.8740(3) \text{ \AA}$, $c = 8.1120(3) \text{ \AA}$, $\alpha = 102.706(2)^\circ$, $\beta = 104.976(2)^\circ$, $\gamma = 92.632(3)^\circ$, $V = 422.61(3) \text{ \AA}^3$, $Z = 2$, $R = 0.0337$ for 1827 observed reflections. The crystal structure is formed by pairs of anions that are mutually connected in chains through two water molecules. These chains are interconnected by biguanidium(2+) cations to form a three-dimensional network.

The FTIR and FT Raman spectra of all five compounds were recorded, calculated (HF, B3LYP and MP2 methods) and discussed.

Quantitative measurements of second harmonic generation of powdered biguanidium(2+) nitrate and novel biguanidium(2+) carbonate monohydrate at 800 nm were performed and a relative efficiency (compared to KDP) of 87% and 20% was observed, respectively. © 2007 Elsevier B.V. All rights reserved.

Keywords: Biguanidium(2+) nitrate; Biguanidium(2+) carbonate monohydrate; Biguanidium(1+) phosphite trihydrate; Biguanidium(2+) phosphite monohydrate; Biguanidium(2+) hydrogen phosphate monohydrate; Crystal structure; Vibrational spectra; Second harmonic generation; HF; B3LYP; MP2

1. Introduction

The structure of biguanide can be derived from biuret by substitution of two oxygen atoms by imino groups. Biguanide is a much stronger base ($pK_{a1} = 11.52$ and

$pK_{a2} = 2.93$) than biuret ($pK_a = 9.61$) and belongs amongst the strongest organic bases. Biguanide and its N-substituted derivatives are widely studied strong σ - and π -donating bidentate ligands, which form stable complexes [1,2] with transition metal ions in high or unusual oxidation states.

Applications of biguanides lie mainly in the area of medical research [3,4], especially in the treatment of diabetes mellitus [5–7]. Biguanide derivatives are also used in the

* Corresponding author. Tel.: +420 221 951 255; fax: +420 221 951 253.
E-mail address: irena.mat@atlas.cz (I. Matulková).

synthesis of antimalarial drugs [8] and in therapeutic treatment of pain, anxiety, memory disorders [9] and hypoglycaemic activity [1,3,10,11].

Moreover, biguanide complexes of boron have also been investigated as potential compounds for wood conservation [12] and crystals of biguanidium dinitramides were studied as promising energetic materials [13–15].

Another application of biguanidium cations, i.e. a rigid skeleton with delocalized π -electrons, lies in the area of preparation of novel nonlinear optical (NLO) materials. Biguanide, as well as guanidine [16], can be employed in material engineering of a promising class of NLO compounds based on salts combining a cation derived from a polarizable organic molecule with an anion capable of forming hydrogen-bonded crystal structures [17]. It is assumed that the organic cations in these salts are mainly responsible for the NLO properties of the crystals. The anionic part (inorganic or organic) of these materials can prevent cations from forming unfavourable centrosymmet-

ric arrangements and are also responsible for favourable chemical, mechanical and thermal properties, due to strong hydrogen bond interactions, which stabilize the crystal lattice [18] and also contribute to the NLO properties of the materials [19,20].

In the group of inorganic salts of biguanide, several crystal structures of the biguanidium(1+) and (2+) salts with nitric, perchloric, sulphuric, and hydrochloric acids have been resolved and reported [21–24]. The crystal structure of biguanidium(1+) carbonate has also been resolved [23] and the formation of biguanidium hydrogen phosphate monohydrate and conclusions (based on powder X-ray diffraction data) concerning crystallographic system and space group have been also mentioned in the literature [25].

This work, which is part of our project focused on preparation and study of novel materials for second harmonic generation (SHG), deals with optical characterization of two non-centrosymmetric salts of biguanide and preparation and study of three novel salts with phosphorous and phos-

Table 1
Basic crystallographic data and structure refinement details for **(bigua)₂HPO₃·3H₂O**, **biguaHPO₃·H₂O** and **biguaHPO₄·H₂O**

Identification code	(bigua)₂HPO₃·3H₂O	biguaHPO₃·H₂O	biguaHPO₄·H₂O
Empirical formula	C ₄ H ₂₃ N ₁₀ O ₆ P	C ₂ H ₁₂ N ₅ O ₄ P	C ₂ H ₁₂ N ₅ O ₅ P
Formula weight	338.29	201.14	217.14
Temperature (K)	293(2)	293(2)	293(2)
<i>a</i> (Å)	7.1740(1)	6.9690(2)	7.0630(2)
<i>b</i> (Å)	9.6530(2)	7.3500(3)	7.8740(3)
<i>c</i> (Å)	11.3140(2)	8.1730(3)	8.1120(3)
α (°)	70.094(1)	82.518(2)	102.706(2)
β (°)	75.688(1)	83.015(2)	104.976(2)
γ (°)	86.099(1)	82.811(3)	92.632(3)
Volume (Å ³)	713.71(2)	409.44(3)	422.61(3)
<i>Z</i>	2	2	2
Calculated density (Mg/m ³)	1.574	1.631	1.706
Crystal system	Triclinic	Triclinic	Triclinic
Space group	<i>P</i> $\bar{1}$	<i>P</i> $\bar{1}$	<i>P</i> $\bar{1}$
Absorption coefficient (mm ⁻¹)	0.241	0.327	0.332
<i>F</i> (000)	360	212	228
Crystal size (mm)	0.50 × 0.40 × 0.40	0.50 × 0.40 × 0.25	0.57 × 0.50 × 0.30
Diffraction and radiation	Nonius Kappa CCD, $\lambda = 0.71073$ Å		
Scan technique	ω and ψ scans to fill the Ewald sphere		
Completeness to θ	27.54 99.0 %	27.52 98.1 %	27.54 98.5 %
Range of <i>h</i> , <i>k</i> and <i>l</i>	-9 → 9, -12 → 12, -14 → 14	-9 → 9, -9 → 9, -10 → 10	-7 → 9, -10 → 10, -10 → 10
θ range for data collection (°)	3.12–27.54	2.81–27.52	2.68–27.54
Reflection collected/unique	17053/3273	5116/1843	4522/1919
(<i>R</i> _{int})	(0.0195)	(0.0232)	(0.0253)
No. of observed reflection	3031	1779	1827
Absorption correction	none		
Function minimised	$\Sigma w(F_o^2 - F_c^2)^2$		
Weighting scheme	$w = [\sigma^2(F_o^2) + (aP)^2 + bP]^{-1}$ $P = (F_o^2 + 2F_c^2)/3$		
Parameters refined	<i>a</i> = 0.0563 <i>b</i> = 0.3593	<i>a</i> = 0.0366 <i>b</i> = 0.2347	<i>a</i> = 0.0349 <i>b</i> = 0.3250
<i>R</i> , <i>wR</i> [<i>I</i> > 2 σ (<i>I</i>)]	0.0350, 0.0983	0.0308, 0.0840	0.0337, 0.0885
<i>R</i> , <i>wR</i> (all data)	0.0376, 0.1009	0.0319, 0.0849	0.0354, 0.0899
Value of <i>S</i>	1.007	1.085	1.074
Max. and min. heights in final $\Delta\rho$ map (e Å ⁻³)	0.487 and -0.450	0.403 and -0.346	0.393 and -0.369
Sources of atomic scattering factors	SHELXL97 [35]		
Programs used	SHELXL97 [35], PLATON [39], SIR97 [34]		

phoric acids. The motivation for utilization of phosphorus oxy-acids was their ability to form a hydrogen-bonded anionic framework, which was successfully employed in preparation of several materials for SHG [17,26,27]. The full assignment of vibrational spectra (employing quantum-chemical computational methods) of the materials is very important, not only for their identification, but also in relation to their nonlinear optical properties. It is very well known that the polarizability and hyperpolarizabilities of molecules is dependent on their electronic structure. However, particular attention has recently been paid to the vibrational contributions to the first and second hyperpolarizabilities (β and γ) of molecules [28–32].

In this paper, the vibrational spectra and optical properties of biguanidium(2+) nitrate (**bigua**(NO₃)₂) and biguanidium(2+) carbonate monohydrate (**bigua**CO₃·H₂O), along with the crystal structures and vibrational spectra of biguanidium(1+) phosphite trihydrate ((**bigua**)₂HPO₃·3H₂O), biguanidium(2+) phosphite monohydrate (**bigua**HPO₃·H₂O) and biguanidium(2+) hydrogen phosphate monohydrate (**bigua**-HPO₄·H₂O), are presented and discussed.

2. Experimental

Crystals of **bigua**CO₃·H₂O were prepared by a slight modification of a procedure described previously in the literature [33]. A mixture of dicyanodiamide (80 g, 0.94 mol, 98%, purum, Fluka), ammonium chloride (120 g, 2.25 mol, p.a., Lachema, dried in a desiccator over KOH for one day) and phenol (250 ml, purum, Lachema) were heated to 140–145 °C in an oil bath for 5.5 h. The reaction mixture was poured into 1000 ml of water and extracted with diethyl ether (500 ml, Lachema) to remove the phenol. The aqueous solution was filtered to remove the by-product (melamine). An aqueous saturated solution of 60 g

CuSO₄·5H₂O was added to the water phase and a pink precipitate was formed. The precipitate was filtered off and the remaining part of the product was precipitated by addition of 25% aqueous ammonia. The whole yield was approximately 95 g (56%) of the copper bis-(biguanide) sulphate complex. The complex was decomposed to biguanidium(2+) sulphate by repeated recrystallization from 10% sulphuric acid solution. The white crystalline solid obtained (biguanidium(2+) sulphate monohydrate) was characterized by elemental analysis: C % 11.29 (11.27), H % 5.24 (5.16) and N % 30.65 (32.86) (the values in the brackets were calculated). The solution of biguanidium(2+) sulphate was mixed with a barium hydroxide solution and the crude barium sulphate formed was filtered off. The filtrate was aerated by gaseous CO₂ and left to crystallize. The obtained **bigua**CO₃·H₂O crystals were filtered off, washed with methanol, dried in a desiccator over KOH and characterized by elemental analysis: C % 20.73 (19.88), H % 5.92 (6.00) and N % 38.64 (38.67).

Crystals of **bigua**(NO₃)₂ were crystallized from a solution obtained by addition of **bigua**CO₃·H₂O to a nitric acid (p.a., Lachema) solution (2 mol l⁻¹) in a 1:2 molar ratio. The white crystalline product was filtered off, washed with methanol, dried in a desiccator over KOH and characterized by elemental analysis: C % 11.42 (10.58), H % 4.10 (3.99) and N % 41.70 (43.17). The product was also characterized by the method of X-ray powder diffraction – the recorded pattern was compared with the calculated diffraction pattern (PLATON software) based on the previously resolved crystal structure [21].

Crystals of (**bigua**)₂HPO₃·3H₂O and **bigua**HPO₃·H₂O were prepared by addition of biguanidium(2+) carbonate monohydrate to a 2 mol l⁻¹ solution of phosphorous acid (purum p.a., Fluka) in a 2: 1 and 1: 1 molar ratio (base: acid), respectively. Similarly, **bigua**HPO₄·H₂O crystals

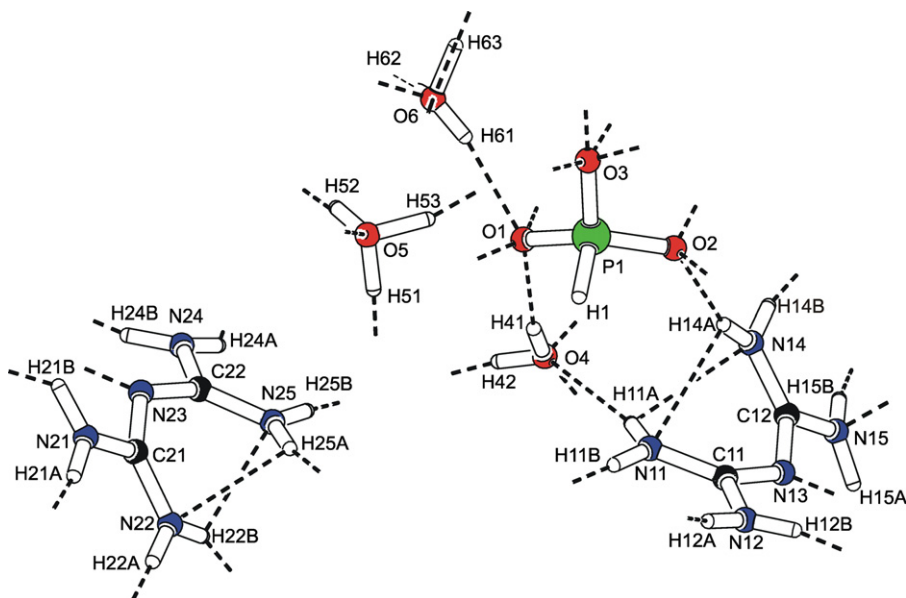


Fig. 1. Atom numbering of (**bigua**)₂HPO₃·3H₂O. Dashed lines indicate hydrogen bonds.

were obtained from 2 mol l⁻¹ phosphoric acid (purum, Lachema) solution (2:1 molar ratio). The colourless solutions obtained were kept in a desiccator over KOH at room temperature. The prepared crystals were filtered off, washed with methanol and dried in a desiccator over KOH.

Collection of X-ray structural data was performed on a Nonius Kappa CCD diffractometer (MoK_α radiation, graphite monochromator). The phase problem was solved by direct methods (SIR-92 [34]) and the non-hydrogen atoms were refined anisotropically, using the full-matrix least-squares procedure (SHELXL-97 [35]). The positions of the hydrogen atoms were localised on difference Fourier maps and were fixed during refinement using rigid body approximation with assigned displacement parameters equal to 1.2 U_{iso} (pivot atom). The basic crystallographic data, measurement and refinement details are summarised in Table 1. Crystallographic data for (bigua)₂HPO₃·3H₂O, biguaHPO₃·H₂O and biguaHPO₄·H₂O have been deposited with the Cambridge Crystallographic Data Centre as supplementary publications CCDC 635150, CCDC 635151 and CCDC 635152, respectively. A copy of the data can be obtained free of charge on application to CCDC, 12 Union Road, Cambridge CB21, EZ, UK (fax: +44 1223 336 033; e-mail: deposit@ccdc.cam.ac.uk).

X-ray powder diffraction patterns were obtained using an URD-6 instrument (Freiberg, CuK_α radiation). The measurements were performed in the range 3–100° 2θ in steps of 0.02° (5 s per step).

The infrared spectra were recorded using DRIFTS and nujol or fluorolube mull (KBr and AgCl windows) techniques on a Nicolet Magna 760 FTIR spectrometer with 2 cm⁻¹ resolution and Happ–Genzel apodization in the 400–4000 cm⁻¹ region. FAR IR spectra were recorded down to 100 cm⁻¹ (4 cm⁻¹ resolution) in PE pellets.

The Raman spectra of polycrystalline samples were recorded on a Nicolet Magna 760 FTIR spectrometer equipped with the Nicolet Nexus FT Raman module (2 cm⁻¹ resolution, Happ–Genzel apodization, 1064 nm Nd:YVO₄ laser excitation, 200 mW power at the sample) in the 100–3700 cm⁻¹ region.

The UV–Vis–NIR spectra of aqueous solutions were recorded in the 190–1100 nm range using a Unicam UV 300 spectrometer.

The quantum-chemical calculations were performed employing the closed-shell restricted Hartree–Fock (HF), Density Functional Theory (B3LYP) and Møller Plesset perturbation (MP2) methods with the 6-311G basis set. For the HF method, quantum-chemical calculation was also performed with the 6-311G(d) and 6-311G(d,p) basis sets. The calculations and visualisation of the results were performed with Gaussian 98W [36] and GaussView 2.1 [37] program packages. The geometry optimisations, also yielding the molecular energies, were followed by frequency calculations, together with IR and Raman intensities, using the same basis set. The calculated geometry and frequencies scaled with precomputed vibrational scaling factors [38] were compared to the experimental values.

The measurements of SHG at 800 nm were performed with 90 fs laser pulses generated at an 82 MHz repetition rate by a Ti:sapphire laser (Tsunami, Spectra Physics). For quantitative determination of the SHG efficiency, the intensity of the back-scattered laser light at 400 nm generated in the sample was measured by a grating spectrograph with diode array (InstaSpec II, Oriel) and the signal was compared with that generated in KDP (i.e. KH₂PO₄). The experiment was performed using a powdered sample (75–150 μm particle size) loaded into 5 mm glass cells with the aid of a vibrator and the measurements were repeated

Table 2
Selected bond lengths [Å] and angles [°] for (bigua)₂HPO₃·3H₂O

Bond/angle	Value	Angle	Value
P1–O2	1.506(1)	O2–P1–O1	113.32(6)
P1–O3	1.514(1)	O3–P1–O1	112.63(7)
P1–O1	1.516(1)	N12–C11–N11	118.7(1)
N11–C11	1.338(2)	N12–C11–N13	116.1(1)
N12–C11	1.325(2)	N11–C11–N13	125.1(1)
C11–N13	1.342(2)	N14–C12–N13	126.8(1)
C12–N14	1.328(2)	N14–C12–N15	117.6(1)
C12–N13	1.328(2)	N13–C12–N15	115.5(1)
C12–N15	1.346(2)	C12–N13–C11	125.3(1)
N21–C21	1.339(2)	N22–C21–N23	126.8(1)
N22–C21	1.328(2)	N22–C21–N21	117.5(1)
C21–N23	1.336(2)	N23–C21–N21	115.6(1)
C22–N25	1.330(2)	N25–C22–N24	118.6(1)
C22–N24	1.337(2)	N25–C22–N23	125.3(1)
C22–N23	1.341(2)	N24–C22–N23	116.1(1)
O2–P1–O3	111.80(6)	C21–N23–C22	123.7(1)

Hydrogen bonds

D–H...A	d(D–H)	d(H...A)	d(D...A)	<(DHA)
N11–H11A...O4W	0.96	2.23	3.135(2)	155.9
N11–H11A...N14	0.96	2.56	2.972(2)	106.3
N11–H11B...O1 ^a	0.89	2.18	3.043(2)	165.2
N12–H12A...O5W ^a	0.89	2.09	2.933(2)	157.7
N12–H12B...N13 ^b	0.84	2.19	3.019(2)	169.1
N14–H14A...N11	0.93	2.57	2.972(2)	106.2
N14–H14A...O2	0.93	1.96	2.850(2)	159.2
N14–H14B...O4W ^d	0.88	2.16	3.027(2)	165.0
N15–H15B...O1 ^c	0.88	2.24	3.103(2)	166.4
N21–H21A...O3 ^d	0.88	2.22	3.090(2)	169.2
N21–H21B...O6W ^e	0.96	2.31	3.050(2)	133.5
N22–H22A...O2 ^d	0.90	1.96	2.854(2)	173.5
N22–H22B...O4W ^f	0.94	2.33	3.193(2)	152.0
N22–H22B...N25	0.94	2.40	2.919(2)	114.6
N24–H24A...O6W ^g	0.88	2.48	3.193(2)	138.3
N24–H24B...N23 ^h	0.92	2.11	3.008(2)	166.7
N25–H25A...O2 ^a	0.97	1.96	2.894(2)	162.7
N25–H25A...N22	0.97	2.49	2.919(2)	106.4
N25–H25B...O3 ^g	0.88	2.04	2.920(2)	173.4
O4W–H41...O1 ^a	0.87	1.94	2.780(2)	161.6
O4W–H42...O3 ^g	0.82	2.21	3.030(2)	172.3
O5W–H52...O6W ⁱ	1.01	1.87	2.870(2)	166.8
O5W–H51...O3 ^g	0.95	1.82	2.770(2)	174.6
O5W–H53...N15	1.05	2.35	3.374(2)	165.0
O6W–H61...O1 ^c	0.81	1.96	2.761(2)	169.1
O6W–H62...O5W ⁱ	0.83	2.08	2.870(2)	158.3

Note. Equivalent positions: (a) $-x + 1, -y + 1, -z + 1$; (b) $-x + 1, -y, -z + 2$; (c) $-x + 1, -y, -z + 1$; (d) $x - 1, y + 1, z$; (e) $-x + 1, -y + 2, -z$; (f) $-x, -y + 1, -z + 1$; (g) $x - 1, y, z$; (h) $-x, -y + 2, -z$; (i) $-x + 1, -y + 1, -z$. Abbreviations: A, acceptor; D, donor.

on different areas of the same sample (the results were averaged). This experimental procedure minimises the signal fluctuations induced by sample packing.

3. Results and discussion

3.1. Crystal structures

The crystals of $(\text{bigua})_2\text{HPO}_3 \cdot 3\text{H}_2\text{O}$ belong in the triclinic system (space group $P\bar{1}$). The atom numbering is depicted in Fig. 1 (PLATON software [39]). The selected bond lengths and angles including those of the hydrogen

bonds are listed in Table 2. The asymmetric unit consists of two biguanidium(1+) cations, a phosphite anion and three water molecules (of which two molecules are disordered – occupation factor of 0.5 is assigned to the positions

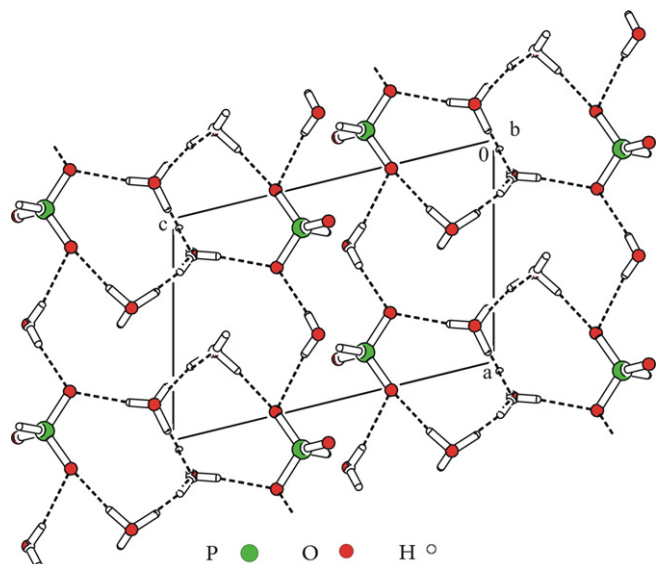


Fig. 2. Network of phosphite anions and molecules of water in the $(\text{bigua})_2\text{HPO}_3 \cdot 3\text{H}_2\text{O}$ structure. Dashed lines indicate hydrogen bonds.

Table 3

Selected bond lengths [Å] and angles [°] for $\text{biguaHPO}_3 \cdot \text{H}_2\text{O}$

Bond/angle	Value	Angle	Value	
P1–O2	1.504(1)	O2–P1–O1	111.45(6)	
P1–O3	1.520(1)	O3–P1–O1	111.39(6)	
P1–O1	1.534(1)	C2–N3–C1	126.2(1)	
N1–C1	1.315(2)	N2–C1–N1	121.6(1)	
N2–C1	1.307(2)	N2–C1–N3	121.9(1)	
N3–C2	1.370(2)	N1–C1–N3	116.5(1)	
N3–C1	1.373(2)	N4–C2–N5	121.8(1)	
N4–C2	1.314(2)	N4–C2–N3	115.7(1)	
N5–C2	1.316(2)	N5–C2–N3	122.5(1)	
O2–P1–O3	113.78(6)			
<i>Hydrogen bonds</i>				
D–H...A	<i>d</i> (D–H)	<i>d</i> (H...A)	<i>d</i> (D...A)	<(DHA)
O4W–H1W...O2 ^a	1.61	1.69	2.734(2)	170.8
O4W–H2W...O4W ^b	0.85	2.03	2.875(3)	176.3
O4W–H3W...O3	1.19	2.07	3.253(2)	173.3
N1–H1A...O2 ^a	0.87	2.02	2.889(2)	176.1
N1–H1B...O1	0.86	2.22	3.068(2)	165.8
N2–H2A...O3 ^a	0.87	1.91	2.776(2)	174.8
N2–H2B...O3 ^c	0.87	2.03	2.876(2)	161.0
N3–H3...O1 ^d	0.95	1.74	2.674(2)	169.1
N4–H4A...O3 ^d	0.91	1.85	2.757(2)	172.9
N4–H4B...O2 ^e	0.79	2.18	2.954(2)	165.7
N5–H5A...O4W ^f	0.80	2.18	2.898(2)	148.1
N5–H5A...N2	0.80	2.41	2.950(2)	125.0
N5–H5B...O1 ^e	0.88	2.00	2.877(2)	175.2

Note. Equivalent positions: (a) $-x+1, -y+1, -z$; (b) $-x+2, -y+1, -z$; (c) $x-1, y+1, z$; (d) $-x+1, -y+1, -z+1$; (e) $-x, -y+1, -z+1$; (f) $x-1, y, z$. Abbreviations: A, acceptor; D, donor.

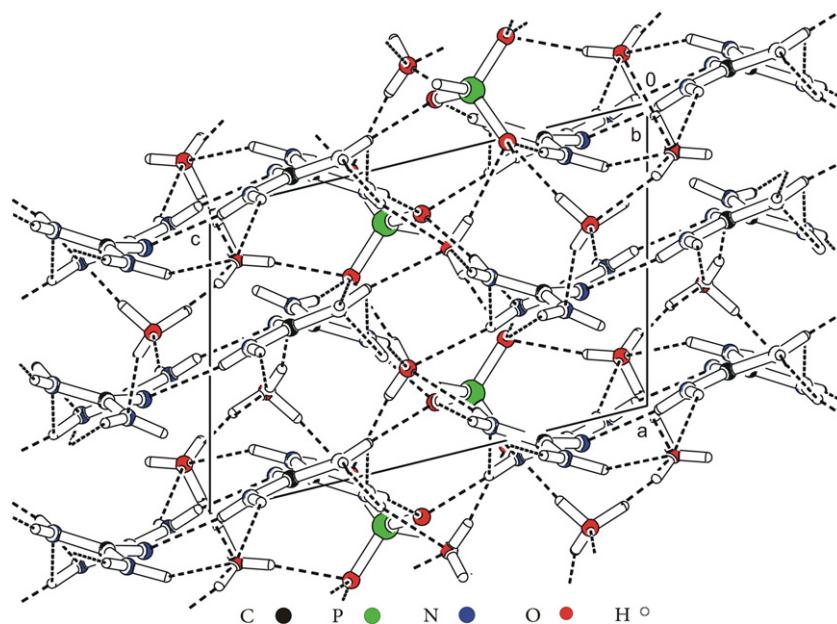


Fig. 3. Packing scheme of the $(\text{bigua})_2\text{HPO}_3 \cdot 3\text{H}_2\text{O}$ (projection to xz plane). Dashed lines indicate hydrogen bonds.

of the H52, H53, H62 and H63 atoms). The basic feature of the crystal structure consists in the network of phosphite anions and water molecules. Chains of alternating anions and water molecules are apparent in this network, and are mutually connected by pairs of water molecules (see Fig. 2). The biguanidium(1+) cations form pairs through two intermolecular hydrogen bonds N12–H12B...N13 and N24–H24B...N23, with lengths of 3.019(2) Å and 3.008(2) Å, and fill the network of anions and water molecules (see Fig. 3). In addition, the conformation of the biguanidium(1+) cations is stabilized by two pairs of intramolecular hydrogen bonds N11–H11A...N14, N14–

H14A...N11 and N22–H22B...N25, N25–H25A...N22 with a donor...acceptor distance of 2.919(2)–2.972(2) Å (see Fig. 1).

The compound **biguaHPO₃·H₂O** crystallises in the triclinic system with the $P\bar{1}$ space group. The bond lengths and angles, including those of the hydrogen bonds, are listed in Table 3 and the atom numbering is depicted in Fig. 4. The asymmetric unit of the crystal structure is formed by a biguanidium(2+) cation, a phosphite anion and a water molecule (which is disordered – occupation factor of 0.5 is assigned to the positions of the H2W and H3W atoms). The entire structure is formed of a network of alternating cations, anions and water molecules (see Fig. 5). The water molecules are interconnected by intermolecular hydrogen bond O4W–H2W...O4W with a length of 2.875(3) Å. The conformation of the individual biguanidium(2+) cations is stabilized by one intramolecular bond N5–H5A...N2 with a donor...acceptor distance of 2.950(2) Å (see Fig. 4).

The salt **biguaHPO₄·H₂O**, which crystallises in the triclinic system, belongs to the $P\bar{1}$ space group. The bond lengths and angles, including those of the hydrogen bonds, are listed in Table 4. The atom numbering is depicted in Fig. 6. The asymmetric unit contains a biguanidium(2+) cation, a hydrogen phosphate anion and a water molecule. The anions form pairs through hydrogen bonds of the O–H...O type, which are mutually joined in chains through two water molecules (see Fig. 7). These chains are interconnected by biguanidium(2+) cations in a three-dimensional

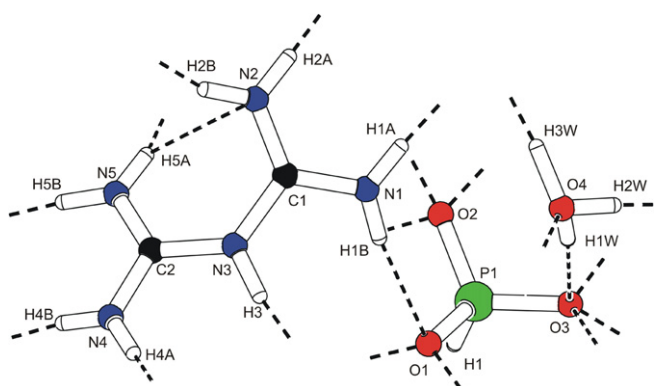


Fig. 4. Atom numbering of **biguaHPO₃·H₂O**. Dashed lines indicate hydrogen bonds.

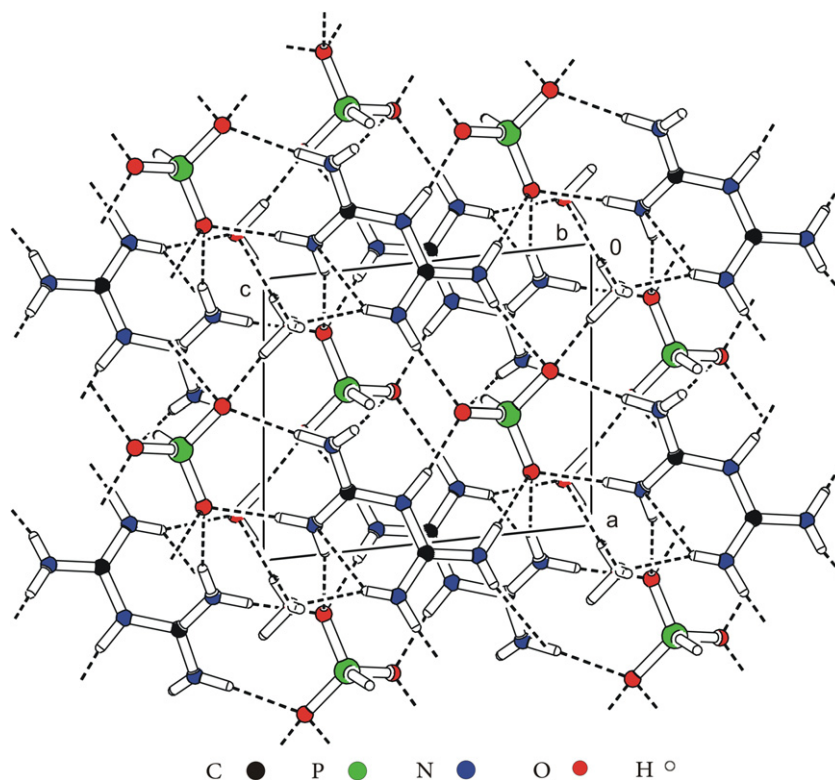


Fig. 5. Packing scheme of **biguaHPO₃·H₂O** (projection to xz plane). Dashed lines indicate hydrogen bonds.

Table 4
Selected bond lengths [\AA] and angles [$^\circ$] for **biguaHPO₄·H₂O**

Bond/angle	Value	Angle	Value
P1–O3	1.496(1)	O4–P1–O2	112.35(7)
P1–O4	1.520(1)	O3–P1–O1	108.9(1)
P1–O2	1.525(1)	O4–P1–O1	107.45(7)
P1–O1	1.579(1)	O2–P1–O1	103.94(7)
N1–C1	1.321(2)	C1–N3–C2	126.8(1)
N2–C1	1.313(2)	N2–C1–N1	121.0(2)
N3–C1	1.367(2)	N2–C1–N3	123.3(2)
N3–C2	1.373(2)	N1–C1–N3	115.6(1)
N4–C2	1.306(2)	N4–C2–N5	122.3(2)
N5–C2	1.321(2)	N4–C2–N3	116.5(2)
O3–P1–O4	112.09(8)	N5–C2–N3	121.1(1)
O3–P1–O2	111.63(8)		

Hydrogen bonds

D–H...A	d(D–H)	d(H...A)	d(D...A)	<(DHA)
O1–H1...O4 ^a	0.91	1.67	2.664(2)	170.1
O5W–H51...O4 ^b	0.90	1.81	2.710(2)	170.3
O5W–H52...O3	0.96	2.10	3.038(2)	165.8
N1–H1A...O4 ^c	0.95	2.17	3.113(2)	171.7
N1–H1A...O3 ^c	0.95	2.66	3.307(2)	126.0
N1–H1B...O2 ^d	0.97	2.00	2.951(2)	166.8
N2–H2B...O1 ^e	0.88	2.30	3.034(2)	140.3
N2–H2B...N5	0.88	2.48	2.948(2)	114.1
N2–H2A...O3 ^e	0.94	1.81	2.727(2)	163.7
N3–H3...O2	0.87	1.83	2.696(2)	170.7
N4–H4A...O3	0.95	1.76	2.709(2)	174.1
N4–H4B...O4 ^f	0.80	2.15	2.946(2)	171.5
N5–H5A...O5W ^g	0.92	1.91	2.824(2)	171.7
N5–H5B...O2 ^f	0.91	2.13	3.014(2)	162.4

Note. Equivalent positions: (a) $-x+2, -y, -z$; (b) $-x+2, -y, -z+1$; (c) $x, y+1, z$; (d) $-x+2, -y+1, -z+1$; (e) $-x+1, -y+1, -z$; (f) $x-1, y, z$; (g) $-x+1, -y+1, -z+1$. Abbreviations: A, acceptor; D, donor.

network (via hydrogen bonds of the N–H...O type with lengths of 2.951(2)–3.307(2) \AA – see Fig. 8). The conformation of the biguanidium(2+) cation is stabilized by one

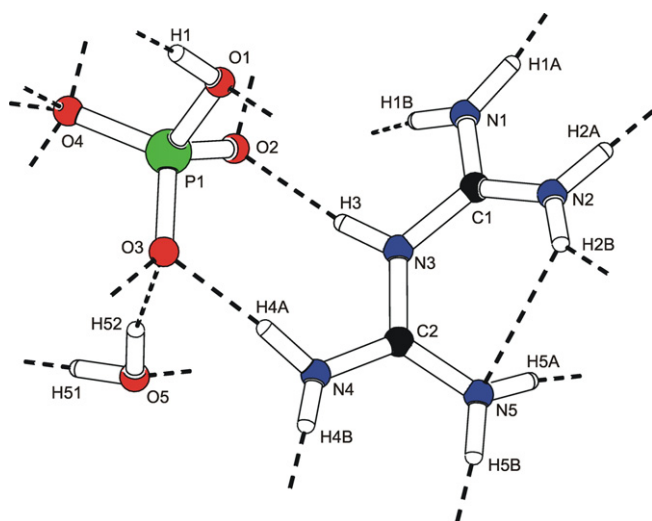


Fig. 6. Atom numbering of **biguaHPO₄·H₂O**. Dashed lines indicate hydrogen bonds.

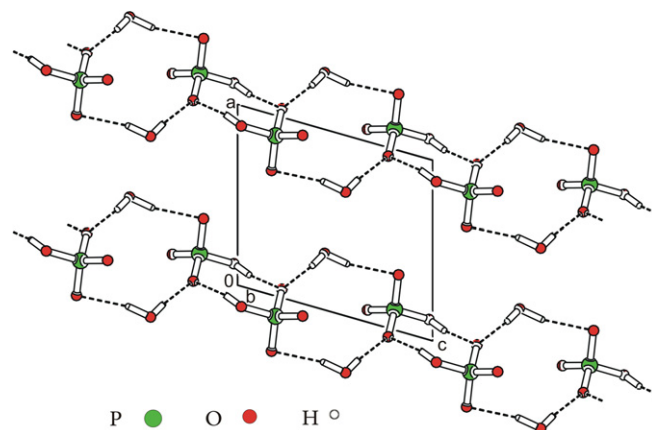


Fig. 7. Network of phosphate anions and molecules of water in the **biguaHPO₄·H₂O** structure. Dashed lines indicate hydrogen bonds.

intramolecular hydrogen bond N2–H2B...N5 with a donor...acceptor distance of 2.948(2) \AA (see Fig. 6).

All the crystal structures of biguanide salts are formed by relatively strong hydrogen bonds involving nitrogen atoms. These intermolecular hydrogen bonds can substantially affect the geometry of the biguanidinium cations. The most obvious change in the cation geometry can be observed in the values of the angles between the two planes (each plane is formed by three nitrogen atoms and one carbon atom) to which the biguanidinium cations can be imaginarily assigned.

In the case of the biguanidium(1+) cation, the angles between these two planes equal 39.5° for chloride, 41.5° or 42.7° for carbonate, and 44.0° or 49.1° for sulphate [23]. The discussed angles equal 38.0° and 36.8° in the (**bigua**)₂HPO₃·3H₂O crystal structure.

In the case of the biguanidium(2+) cation, the inter-planar angles attain values of 43.7°, 47.1° and 48.0° for perchlorate, nitrate and sulphate, respectively [21–23]. The values of 43.5° and 41.8° were found for the described salts **biguaHPO₃·H₂O** and **biguaHPO₄·H₂O**, respectively.

It was found in general that, as the value of the discussed angle between the planes in the biguanide cations increases, the C–N bonding distances also slightly increase.

3.2. Cation geometry optimisation and calculation of vibrational frequencies

In order to assign the vibrational manifestations of biguanidium(1+) and biguanidium(2+) cations, computational geometry optimisation followed by vibrational frequency calculations were performed. The geometry of the isolated biguanidium cations was optimised using closed-shell restricted HF, B3LYP and MP2 methods for the 6-311G basis set. 6-311G(d) and 6-311G(d,p) basis sets were also used for the HF method. Comparison of the experimental (crystal structures) and the calculated values of the geometry-optimized structures is presented in Tables 5 and 6. According to this comparison, the best results were

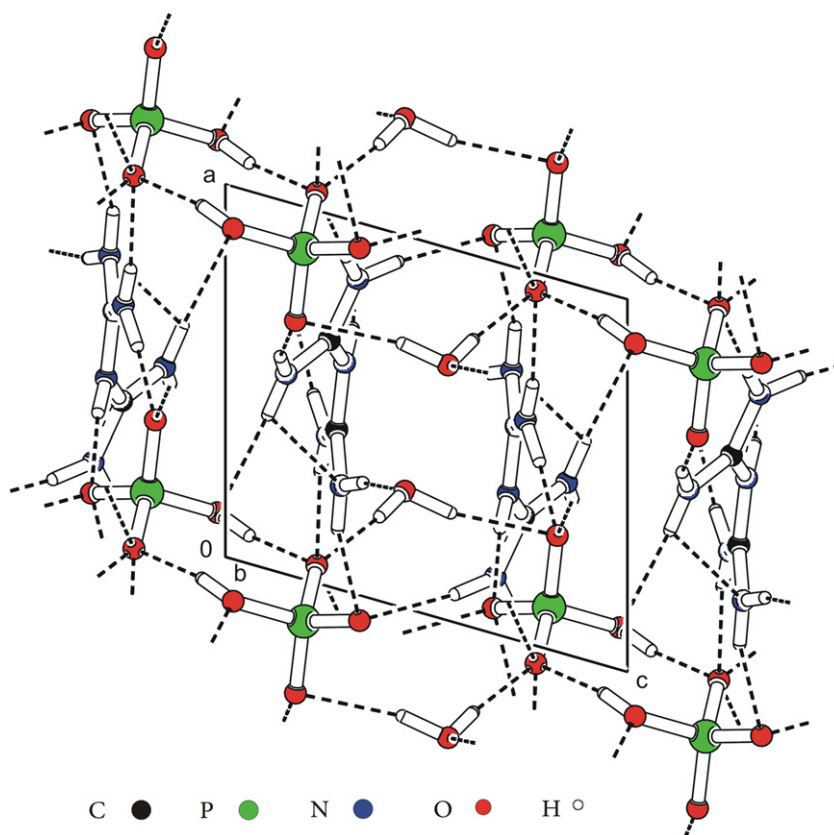


Fig. 8. Packing scheme of **biguaHPO₄·H₂O** (projection to *xz* plane). Dashed lines indicate hydrogen bonds.

obtained for the HF method for both calculated species. In the case of the MP2 (both cations) and B3LYP (dication only) methods, all the bond lengths are systematically slightly overestimated. The values of the inter-atomic angles fluctuate slightly around the values obtained in the crystal structure determinations.

The results of fundamental vibrational frequency calculations, together with the experimental data for biguanidium(1+) and biguanidium(2+) chlorides, are presented in Tables 7 and 8, respectively. The intensities of the calculated IR and Raman bands are presented on a relative scale from 0 to 100. The proposed assignment of the vibrational bands is based on visualisation of the atom motions in the GaussView [37] program. The best match with the recorded spectra was obtained for the scaled HF/6-311G(d,p) method. The largest differences between the calculated and recorded peak positions were observed for the stretching N–H vibrations, because the formation of hydrogen bonds, which strongly affects the positions and intensities of the bands, was not considered in the calculations.

3.3. Vibrational spectra

The FTIR and FT Raman spectra of **(bigua)₂HPO₃·3H₂O**, **bigua(NO₃)₂**, **biguaCO₃·H₂O**, **biguaHPO₃·H₂O** and **biguaHPO₄·H₂O** recorded at room temperature are depicted in Figs. 9–13, respectively. The assignment

of the observed bands (Tables 9,11,13–15) is based on ab initio calculations (HF/6-311G(d,p)) of biguanidium(1+) and biguanidium(2+) cations and previous papers concerning the vibrational spectra of phosphites and phosphates [40–43].

3.3.1. Vibrational spectra of biguanidium(1+) salt – **(bigua)₂HPO₃·3H₂O**

Broad structured bands in the 3600–3100 cm⁻¹ region in both spectra correspond to the vibrational manifestations of the N–H and O–H groups participating in the hydrogen bonds of the N–H...O (with lengths of 2.85–3.19 Å) and O–H...O (with lengths of 2.76–3.03 Å) types. Strong broad bands in the 3000–2700 cm⁻¹ region in the IR spectrum can be assigned to the stretching vibrations of N–H groups participating in N–H...N hydrogen bonds with lengths of 2.76–3.02 Å. The recorded positions of the bands corresponding to the O–H and N–H stretching vibrations are in agreement with the curves [44,45] correlating the position of vibrational bands with the length of the appropriate hydrogen bonds found in the crystal structure. Manifestations of out-of-plane bending mode γ O–H(...O) can be assigned to the intense band at 600 cm⁻¹ in the IR spectrum.

It is almost impossible to distinguish biguanidium(1+) and biguanidium(2+) cations in the studied salts by the methods of vibrational spectroscopy. Perhaps a slight indication of the presence of the biguanidium(1+) cation are the

Table 5
Experimental and calculated bond lengths and angles for **biguanidium(1+)** cation

X-ray data for (bigua)₂HPO₃·3H₂O						Geometry optimization							
Bond	cation 1 (Å)	cation 2 (Å)	Angle	cation 1 (°)	cation 2 (°)	B3LYP/6-311G		MP2/6-311G		HF/6-311G		HF/6-311G(d,p)	
						Bond (Å)	Angle (°)	Bond (Å)	Angle (°)	Bond (Å)	Angle (°)	Bond (Å)	Angle (°)
N(1)–C(1)	1.338(2)	1.339(2)	C(1)–N(1)–H(1A)	121.20	121.00	1.345	123.54	1.348	123.36	1.328	123.29	1.323	122.78
N(1)–H(1A)	0.9621	0.8847	C(1)–N(1)–H(1B)	116.90	118.50	1.000	117.97	1.000	117.74	0.980	118.16	0.993	118.14
N(1)–H(1B)	0.8884	0.958	H(1A)–N(1)–H(1B)	119.60	120.20	1.000	118.34	1.000	118.35	0.990	118.42	0.993	118.83
N(2)–C(1)	1.325(2)	1.328(2)	C(1)–N(2)–H(2A)	116.50	116.50	1.360	121.93	1.360	121.15	1.340	121.45	1.345	119.99
N(2)–H(2A)	0.8933	0.8956	C(1)–N(2)–H(2B)	116.20	117.80	1.000	120.58	1.000	120.02	0.990	121.13	0.995	119.45
N(2)–H(2B)	0.8426	0.9418	H(2A)–N(2)–H(2B)	124.50	124.50	1.000	116.60	1.000	116.56	0.980	116.56	0.994	116.05
N(3)–C(2)	1.328(2)	1.341(2)	C(2)–N(3)–C(1)	125.3(1)	123.7(1)	1.330	128.21	1.350	125.25	1.320	128.79	1.316	126.11
N(3)–C(1)	1.342(2)	1.336(2)	C(2)–N(4)–H(4A)	121.70	116.40	1.330	117.97	1.350	117.74	1.320	118.17	1.316	119.48
N(4)–C(2)	1.328(2)	1.337(2)	C(2)–N(4)–H(4B)	117.20	113.40	1.340	123.54	1.340	123.36	1.320	123.30	1.341	120.02
N(4)–H(4A)	0.9319	0.8825	H(4A)–N(4)–H(4B)	117.20	126.30	1.000	118.33	1.000	118.35	0.990	118.40	0.994	116.06
N(4)–H(4B)	0.8848	0.9153	C(2)–N(5)–H(5A)	115.60	121.20	1.000	120.59	1.000	120.02	0.980	121.13	0.995	122.77
N(5)–C(2)	1.346(2)	1.330(2)	C(2)–N(5)–H(5B)	122.10	116.50	1.360	121.92	1.360	121.15	1.340	121.44	1.323	118.14
N(5)–H(5A)	0.9131	0.9674	H(5A)–N(5)–H(5B)	119.70	121.40	1.000	116.60	1.000	116.55	0.980	116.58	0.993	118.84
N(5)–H(5B)	0.8815	0.88	N(2)–C(1)–N(1)	118.7(1)	117.5(1)	1.000	118.51	1.000	118.64	0.990	118.44	0.994	117.97
			N(2)–C(1)–N(3)	116.1(1)	126.8(1)		124.37		124.81		124.62		125.15
			N(1)–C(1)–N(3)	125.1(1)	115.6(1)		117.06		116.52		116.89		116.87
			N(4)–C(2)–N(5)	117.6(1)	118.6(1)		118.51		118.64		118.44		117.98
			N(4)–C(2)–N(3)	126.8(1)	116.1(1)		117.06		116.52		116.88		116.86
			N(5)–C(2)–N(3)	115.5(1)	125.3(1)		124.38		124.81		124.62		125.16

Table 6
Experimental and calculated bond lengths and angles for **biguanidium(2+)** cation

X-ray data for biguaHPO₃H₂O and biguaHPO₄H₂O						Geometry optimisation							
						B3LYP/6-311G		MP2/6-311G		HF/6-311G		HF/6-311G(d,p)	
Bond	(Å)	(Å)	Angle	(°)	(°)	Bond	Angle	Bond	Angle	Bond	Angle	Bond	Angle
	biguaHPO₃H₂O	biguaHPO₄H₂O		biguaHPO₃H₂O	biguaHPO₄H₂O	(Å)	(°)	(Å)	(°)	(Å)	(°)	(Å)	(°)
N(1)–C(1)	1.315(2)	1.321(2)	C(1)–N(1)–H(1A)	118.30	121.50	1.327	121.9	1.332	121.75	1.310	121.78	1.302	121.30
N(1)–H(1A)	0.8723	0.9477	C(1)–N(1)–H(1B)	116.00	118.20	1.010	122.58	1.010	122.08	0.990	122.72	1.001	122.20
N(1)–H(1B)	0.8639	0.9707	H(1A)–N(1)–H(1B)	124.60	119.10	1.010	115.5	1.010	116.15	0.990	115.48	0.999	116.45
N(2)–C(1)	1.307(2)	1.313(2)	C(1)–N(2)–H(2A)	118.10	118.80	1.330	121.42	1.330	121.24	1.310	121.11	1.308	120.45
N(2)–H(2A)	0.873	0.9416	C(1)–N(2)–H(2B)	122.70	122.00	1.010	122.66	1.010	122.25	0.990	122.99	1.001	122.12
N(2)–H(2B)	0.875	0.8804	H(2A)–N(2)–H(2B)	119.10	118.50	1.000	115.53	1.010	116.02	0.990	115.45	0.998	116.23
N(3)–C(2)	1.370(2)	1.373(2)	C(2)–N(3)–C(1)	126.2(1)	126.8(1)	1.390	128.37	1.400	127.11	1.380	122.26	1.379	129.23
N(3)–C(1)	1.373(2)	1.367(2)	C(2)–N(3)–H(3)	116.50	118.80	1.390	115.8	1.400	116.44	1.380	115.51	1.379	115.38
N(3)–H(3)	0.9464	0.8731	C(1)–N(3)–H(3)	117.30	113.50	1.010	115.82	1.010	116.44	0.990	115.54	1.001	115.39
N(4)–C(2)	1.314(2)	1.306(2)	C(2)–N(4)–H(4A)	121.40	118.10	1.320	122.58	1.330	122.09	1.310	122.72	1.308	122.12
N(4)–H(4A)	0.9098	0.953	C(2)–N(4)–H(4B)	118.70	127.10	1.010	121.9	1.010	121.75	0.990	121.78	0.998	120.44
N(4)–H(4B)	0.7944	0.799	H(4A)–N(4)–H(4B)	119.40	112.00	1.010	115.5	1.010	116.14	0.990	115.48	1.001	116.22
N(5)–C(2)	1.316(2)	1.321(2)	C(2)–N(5)–H(5A)	113.70	121.30	1.330	122.66	1.330	122.25	1.310	122.99	1.302	121.30
N(5)–H(5A)	0.8049	0.921	C(2)–N(5)–H(5B)	116.50	117.20	1.000	121.42	1.010	121.24	0.990	121.12	1.001	122.21
N(5)–H(5B)	0.8783	0.9101	H(5A)–N(5)–H(5B)	129.70	117.80	1.010	115.53	1.010	121.24	0.990	115.44	0.999	116.44
			N(2)–C(1)–N(1)	121.6(1)	121.0(2)				122.42		122.77		122.44
			N(2)–C(1)–N(3)	121.9(1)	123.3(2)				120.34		119.97		120.66
			N(1)–C(1)–N(3)	116.5(1)	115.6(1)				117.21		117.22		117.06
			N(4)–C(2)–N(5)	121.8(1)	122.3(2)				122.42		122.78		122.26
			N(4)–C(2)–N(3)	115.7(1)	116.5(1)				117.2		117.21		117.05
			N(5)–C(2)–N(3)	122.6(1)	121.1(1)				120.36		119.98		120.67

Table 7

Calculated and experimental fundamental frequencies of biguanidium(1+) cation

B3LYP		MP2		HF		Measured				
6-311G	IR/Raman	6-311G	IR/Raman	6-311G	IR/Raman	6-311G(d,p)	IR/Raman	biguanidium(1+) chloride		
S.F. ^a 0.966	intensities	S.F. ^a 0.950	intensities	S.F. ^a 0.904	intensities	S.F. ^a 0.909	intensities	Assignment	IR	Raman
80	0/1	81	0/1	90	0/1	86	0/1	τ CN ₂		
118	1/0	106	0/0	132	1/0	125	1/0	γ CNC		124 m
167	0/0	185	0/0	176	0/0	202	0/0	δ CNC		239 m
281	2/0	204	4/0	339	1/0	322	6/0	γ CNH, τ NH ₂	250 w	
375	0/1	308	0/0	397	0/1	342	4/0	ω NH ₂		
399	0/1	390	0/2	422	0/0	349	0/0	ω NH ₂ , γ CNH		
439	2/1	391	2/1	441	2/1	405	0/1	δ CN ₃		
509	2/0	421	4/1	527	0/0	430	13/0	δ CN ₃ , ω NH ₂		426 w
524	1/0	490	6/1	537	2/0	459	7/1	γ CNH, ω NH ₂	450 w	456 s
575	4/1	503	31/0	587	2/1	478	24/0	γ CNH, ω NH ₂		
607	14/0	519	6/1	619	0/1	532	0/0	δ CN ₃ , γ CNH		
609	0/1	561	2/1	631	14/0	536	10/2	ω NH ₂ , τ NH ₂		552 w
641	0/1	574	2/0	660	11/0	598	1/0	τ NH ₂ , γ CNC	575 w	575 m
644	21/0	576	0/1	669	0/1	612	1/0	τ NH ₂ , δ CNC, δ CN ₃		
669	8/0	594	11/0	692	5/0	634	1/1	τ NH ₂ , δ CNC, δ CN ₃		646 w
727	33/0	632	10/1	775	6/2	740	5/0	π CN ₃ in phase, γ CNH	731 w	743 m
735	7/2	667	0/4	779	40/0	750	0/3	π CN ₃ out of phase, γ CNH	767 w	
823	1/7	814	0/10	835	3/4	881	1/5	δ CNC, ν CN, ρ NH ₂	910 w	912 s
1003	2/1	989	2/1	1015	2/1	1014	1/0	ν CN ₃ , ρ NH ₂		1007 w
1043	1/1	1049	1/0	1069	1/1	1046	1/1	ρ NH ₂ , ν CN ₃	1047 w	1046 w
1049	1/0	1056	1/0	1072	1/0	1057	2/0	ρ NH ₂ , ν CN ₃	1070 w	1070 w
									1078 sh	
1064	0/3	1067	0/5	1082	0/3	1078	0/2	ρ NH ₂ , ν_s CNC, ν CN ₃	1108 w	1108 m
									1157 w	
1211	0/0	1196	1/0	1228	1/0	1212	1/0	ρ NH ₂ , ν_{as} CNC, ν CN ₃	1217 w	1230 w
1479	7/0	1472	5/0	1480	9/1	1460	6/0	ν CN ₃ , δ CN ₃ , δ NH ₂	1468 m	1470 w
1492	21/0	1483	17/1	1504	22/2	1506	15/0	δ CNC, ν CN ₃ , δ CN ₃ , δ NH ₂	1520 m	1528 m
1548	1/3	1535	100/3	1561	1/2	1544	5/3	ν_s CNC, ν CN ₃ , δ CN ₃ , δ CNH	1536 sh	1540 m
									1560 sh	1557 m
1595	100/0	1540	2/4	1573	100/4	1565	100/3	ν_{as} CNC, ν CN ₃ , δ CN ₃ , δ CNH	1577 s	
1639	22/2	1649	15/3	1657	14/4	1638	33/5	δ NH ₂ , ν CN ₃ , δ CN ₃	1620 sh	1619 w
									1630 s	1637 m
									1667 s	
1646	26/1	1656	19/2	1665	22/3	1653	33/3	δ NH ₂ , ν CN ₃ , δ CN ₃ , δ CNC		
1668	12/0	1677	10/1	1689	7/1	1659	14/1	δ NH ₂ , ν CN ₃ , δ CN ₃ , ν_{as} CNC		
1677	1/1	1684	1/1	1699	2/1	1672	0/0	δ NH ₂ , ν CN ₃ , δ CN ₃ , ν_s CNC		
3467	7/9	3392	12/7	3453	8/5	3456	13/6	ν_s NH ₂		
3467	11/6	3392	4/15	3454	10/3	3457	8/7	ν_s NH ₂		
3474	12/11	3400	13/13	3460	9/13	3466	13/11	ν_s NH ₂		
3478	1/100	3404	1/100	3464	0/100	3470	1/100	ν_s NH ₂		
3586	6/14	3519	6/13	3572	6/13	3565	6/12	ν_{as} NH ₂		
3587	1/8	3520	0/9	3572	1/6	3566	5/12	ν_{as} NH ₂		
3598	5/14	3534	5/5	3582	6/16	3584	9/8	ν_{as} NH ₂		
3599	5/22	3534	4/32	3583	5/22	3584	8/29	ν_{as} NH ₂		

Note. Calculated IR and Raman intensities are presented in relative scale (from 0 to 100). Abbreviations and Greek symbols: ν , stretching; δ , deformation or in-plane bending; γ , π , out-of-plane bending; ω , wagging; τ , torsion; ρ , rocking; s, symmetric; as, antisymmetric.

Table 8
Calculated and experimental fundamental frequencies of biguanidium(2+) cation

B3LYP		MP2		HF		Measured				
6-311G S.F. ^a 0.966	IR/Raman intensities	6-311G S.F. ^a 0.950	IR/Raman intensities	6-311G S.F. ^a 0.904	IR/Raman intensities	6-311G(d,p) S.F. ^a 0.904	IR/Raman intensities	biguanidium(2+) chloride		
								Assignment	IR	Raman
76	0/2	71	0/4	84	0/3	84	0/2	τ C-(NH ₂) ₂		
110	1/1	104	1/1	104	1/0	98	1/0	γ C-N-C		
194	0/1	187	0/2	203	0/1	205	0/1	δ C-N-C		205 m
389	0/2	376	0/3	392	1/1	384	3/1	γ CNH, τ NH ₂	250 w	256 m
399	0/0	398	1/1	394	0/2	396	0/1	δ CN ₃		
426	0/1	431	0/2	431	0/1	426	2/0	γ CNH, τ NH ₂	430 w	423 s
472	0/2	479	0/3	471	0/1	466	0/1	ω NH ₂ , γ CNH, γ NH		
517	1/1	510	1/2	511	1/2	476	1/1	τ NH ₂ , γ CNC		
570	0/1	536	0/1	561	0/0	532	7/1	δ CN ₃ , γ CNH	540 s	552 s
572	1/0	541	0/0	583	0/1	575	16/0	ω NH ₂ , τ NH ₂ , γ NH	575 s	
619	6/1	593	10/0	613	12/1	580	2/1	γ CNH, ω NH ₂		
619	12/0	594	1/1	620	1/2	593	5/0	γ CNH, ω NH ₂		
681	2/4	635	28/0	691	2/4	594	43/0	ω NH ₂ , γ NH, γ CNH		
706	0/0	652	1/8	729	1/0	624	17/2	γ CNH, τ NH ₂		627 m
745	18/0	662	54/1	763	8/0	635	23/0	γ CNH, γ CNC	670 m	
787	3/0	699	2/1	809	1/0	642	16/1	γ CNH, δ CNC		690 w
817	100/0	713	88/0	856	100/0	713	14/0	π CN ₃ in phase, γ CNH	710 m	722 m
829	45/0	726	98/0	858	31/1	717	0/3	π CN ₃ out of phase, γ CNH	775 sh	785 w
910	1/5	895	0/11	918	2/6	922	0/6	δ CNC, ν CN, ρ NH ₂	945 w	946 s
1034	3/3	1008	7/8	1042	2/3	1047	3/1	ν CN ₃ , ρ NH ₂		1008 w
1080	0/1	1080	1/1	1098	1/1	1062	1/1	ρ NH ₂ , ν CN ₃	1070 m	1069 s
1081	1/0	1081	1/1	1100	1/0	1069	0/2	ρ NH ₂ , ν CN ₃		1088 m
1094	0/9	1090	0/16	1112	0/7	1093	0/7	ρ NH ₂ , ν_{as} CNC, ν CN ₃	1105 m	1110 m
1124	2/0	1125	3/0	1145	2/0	1115	4/0	ρ NH ₂ , ν_{as} CNC, ν CN ₃	1153 m	1148 w
1432	10/0	1429	26/0	1438	13/0	1408	15/0	ρ NH ₂ , ν_{s} CNC, ν CN ₃	1419 m	1421 w
									1459 m	
1500	76/2	1490	100/4	1517	54/2	1504	47/2	ν CN ₃ , δ CN ₃ , δ NH ₂	1528 m	1520 m
1515	3/11	1500	4/23	1539	1/9	1530	1/9	ν_{s} CNC, ν CN ₃ , δ CN ₃ , δ CNH	1544 m	1549 m
1613	2/4	1604	11/5	1614	16/0	1577	2/2	δ CNC, ν CN ₃ , δ CN ₃ , δ NH ₂		1584 m
1634	9/1	1626	19/1	1655	14/1	1612	21/0	δ NH ₂ , ν CN ₃ , δ CN ₃		1617 m
1681	53/2	1681	85/2	1688	68/7	1660	38/3	δ NH ₂ , ν CN ₃ , δ CN ₃ , δ CNC	1663 s	
1686	74/1	1685	96/1	1690	58/7	1671	7/2	δ NH ₂ , δ NH, ν CN ₃ , δ CN ₃ , ν_{as} CNC	1690 sh	1690 w
1690	4/1	1688	1/1	1708	0/1	1699	100/3	δ NH ₂ , δ NH, ν CN ₃ , δ CN ₃ , ν_{as} CNC	1705 sh	1710 w
1697	25/1	1690	35/1	1713	8/1	1708	66/3	δ NH ₂ , ν CN ₃ , δ CN ₃ , δ CNC	1725 sh	
3407	39/10	3331	72/15	3391	25/13	3391	34/9	ν_{s} NH ₂		
3408	1/12	3332	60/19	3392	31/11	3392	44/7	ν_{s} NH ₂		
3422	1/19	3346	44/27	3406	23/26	3408	39/21	ν_{s} NH ₂		
3424	28/27	3351	25/100	3408	15/85	3412	15/100	ν_{s} NH ₂		
3434	2/100	3368	18/65	3423	6/100	3434	13/64	ν_{s} NH ₂		
3516	16/13	3454	18/32	3503	13/16	3594	19/7	ν_{as} NH ₂		
3516	15/21	3454	32/11	3503	13/25	3504	24/27	ν_{as} NH ₂		
3527	12/17	3464	2/21	3511	4/20	3510	8/20	ν_{as} NH ₂		
3528	18/19	3464	46/27	3512	25/32	3512	41/28	ν_{as} NH ₂		

^aPrecomputed vibrational scaling factor [38].

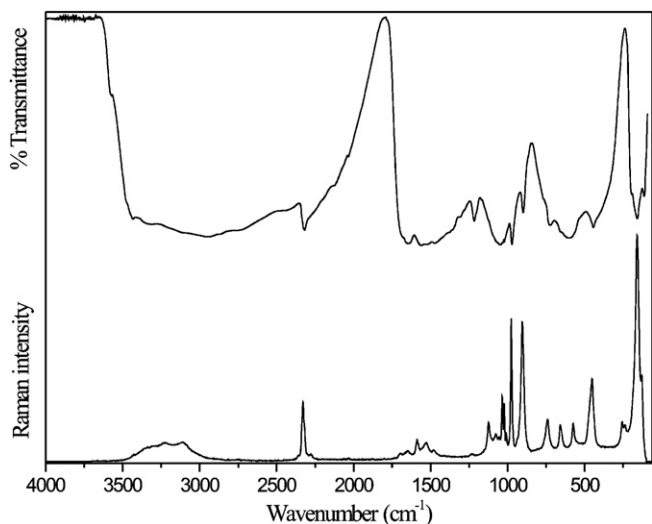


Fig. 9. FTIR (compiled from nujol and fluorolube mulls) and FT Raman spectra of $(\text{bigua})_2\text{HPO}_3 \cdot 3\text{H}_2\text{O}$.

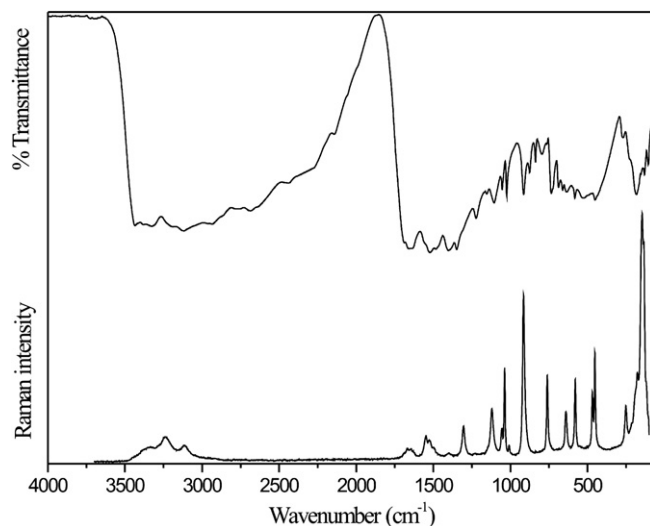


Fig. 11. FTIR (compiled from nujol and fluorolube mulls) and FT Raman spectra of $\text{biguaCO}_3 \cdot \text{H}_2\text{O}$.

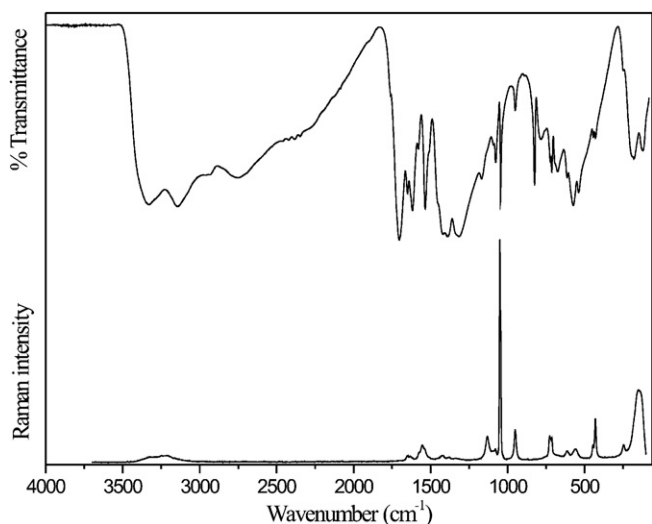


Fig. 10. FTIR (compiled from nujol and fluorolube mulls) and FT Raman spectra of $\text{bigua}(\text{NO}_3)_2$.

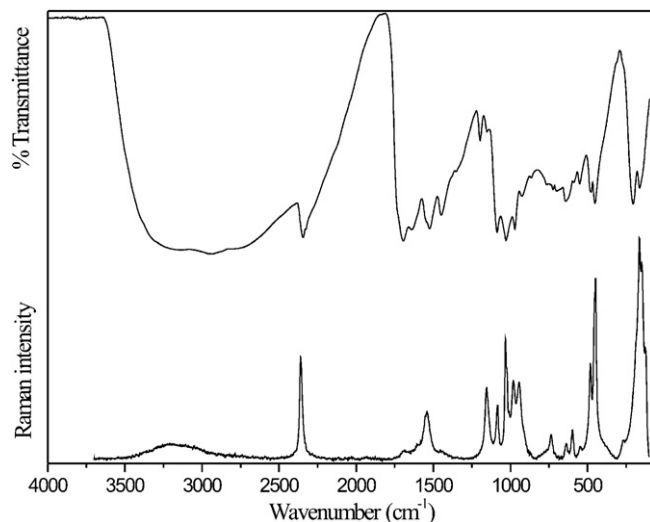


Fig. 12. FTIR (compiled from nujol and fluorolube mulls) and FT Raman spectra of $\text{biguaHPO}_3 \cdot \text{H}_2\text{O}$.

Raman bands at 1663 cm^{-1} (mixed vibrations of $\delta\text{ NH}_2$, $\nu\text{ CN}_3$, $\delta\text{ CN}_3$, $\delta\text{ CNC}$) and 1587 cm^{-1} (mixed vibrations of $\nu_{\text{as}}\text{ CNC}$, $\nu\text{ CN}_3$, $\delta\text{ CN}_3$, $\delta\text{ CNH}$) along with strong IR bands at 1560 cm^{-1} (mixed vibrations of $\nu_{\text{s}}\text{ CNC}$, $\nu\text{ CN}_3$, $\delta\text{ CN}_3$, $\delta\text{ CNH}$) and 1475 cm^{-1} (mixed vibrations of $\nu\text{ CN}_3$, $\delta\text{ CN}_3$, $\delta\text{ NH}_2$). Table 9 gives the assignment of the other vibrational bands of the biguanidium(1+) skeleton.

The sharp, medium-intense band at 2318 cm^{-1} in the IR spectrum and 2329 cm^{-1} in the Raman spectrum is characteristic for the manifestations of stretching vibrations of the P–H group ($\nu_1\text{ HPO}_3^{2-}$). Manifestations of the degenerate $\nu_3''\text{ HPO}_3^{2-}$ vibration were found as a shoulder at 1075 cm^{-1} in the IR spectrum and as a weak band in the Raman spectrum. The bands in the $1050\text{--}1020\text{ cm}^{-1}$ region (slightly overlapping with the $\rho\text{ NH}_2$, $\nu\text{ CN}_3$ vibrations) can be assigned to manifestations of the P–H deformation vibrations ($\nu_2\text{ HPO}_3^{2-}$). The strong band at 976 cm^{-1} in

the Raman spectrum (973 cm^{-1} IR) corresponds to the $\nu_3'\text{ HPO}_3^{2-}$ vibration. The intense bands in the $600\text{--}575\text{ cm}^{-1}$ region can be assigned to phosphite deformation vibrations ν_4' , which overlap with the $\gamma\text{ O-H}(\dots\text{O})$ (IR spectrum) and the $\tau\text{ NH}_2$, $\gamma\text{ CNC}$ (Raman spectrum) vibrations. The strong Raman band at 452 cm^{-1} (444 cm^{-1} IR) was assigned to degenerate $\nu_4''\text{ HPO}_3^{2-}$ deformation vibrations. The above-described vibrational manifestations of the phosphite anion are almost in accordance with the results of performed factor-group analysis presented in Table 10.

3.3.2. Vibrational spectra of biguanidium(2+) salts – $\text{bigua}(\text{NO}_3)_2$, $\text{biguaCO}_3 \cdot \text{H}_2\text{O}$, $\text{biguaHPO}_3 \cdot \text{H}_2\text{O}$ and $\text{biguaHPO}_4 \cdot \text{H}_2\text{O}$

Broad, strong to medium-intense bands located in the $3500\text{--}2400\text{ cm}^{-1}$ region in the IR spectra of all biguanidi-

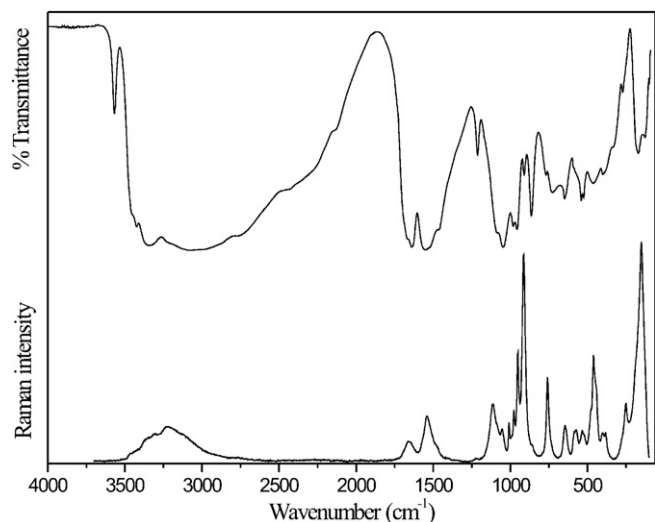


Fig. 13. FTIR (compiled from nujol and fluorolube mulls) and FT Raman spectra of **biguaHPO₄·H₂O**.

um(2+) salts correspond to manifestations of stretching vibrations of N–H groups participating in N–H...O and N–H...N hydrogen bonds. The bands of O–H stretching vibrations (involved in O–H...O hydrogen bonds) should also be expected in this region for the **biguaCO₃·H₂O**, **biguaHPO₃·H₂O** and **biguaHPO₄·H₂O** salts. The recorded positions of the bands discussed for salts with resolved crystal structure are in agreement with the above-mentioned correlation curves [44,45] concerning the N–H or O–H vibrational bands and the lengths of appropriate hydrogen bonds. The bands of the relevant out-of-plane

bending modes (i.e. γ N–H(...O) and γ O–H(...O)) were observed in the IR spectra in the 880–640 cm^{-1} region.

As was mentioned for the biguanidium(1+) cation, it is difficult to find vibrational markers only for the biguanide dication, especially in this group of salts, which vary slightly in the conformation of the cation and radically in its participation in the system of hydrogen bonds. The assignment of the vibrational bands of the biguanidium(2+) skeleton in individual salts is given in Tables 11, 13, 14 and 15.

A pair of strong broad bands at 1388 and 1317 cm^{-1} in the IR spectrum of **bigua(NO₃)₂** (weak Raman bands at 1380 and 1335 cm^{-1}) corresponds to the ν_3 nitrate vibrations. Dominant, very strong bands at 1051 and 1044 cm^{-1} in the Raman spectrum (1045 cm^{-1} IR) were assigned to the symmetric stretching vibrations of the anion (ν_1 NO₃[−]). Splitting of this band in the Raman spectrum is probably the result of the presence of two independent anions in the asymmetric unit. The medium-intense band at 825 cm^{-1} , which was recorded only in the IR spectrum, can be assigned to the ν_2 NO₃[−] vibrations. Doublets at 723 and 713 cm^{-1} (IR) or 726 and 713 cm^{-1} (Raman) were assigned to the ν_4 NO₃[−] vibrations mixed with manifestations of cation π CN₃, γ CNC vibrations. The expected level of factor group splitting (see Table 12) was not observed in the vibrational spectra of **bigua(NO₃)₂**.

Strong, IR active bands observed in the spectra of **biguaCO₃·H₂O** in the 1400–1350 cm^{-1} region are characteristic for ν_3 carbonate vibrations. The strong Raman band located at 1037 cm^{-1} corresponds to the symmetric stretching vibration (ν_1 CO₃^{2−}). Medium intensity bands recorded

Table 9
FTIR and FT Raman spectra of **(bigua)₂HPO₃·3H₂O**

IR (cm^{-1})	Raman (cm^{-1})	Assignment	IR (cm^{-1})	Raman (cm^{-1})	Assignment
3575 vw		ν N–H(...O), ν O–H(...O)	1217 m		ρ NH ₂ , ν_{as} CNC, ν CN ₃
3435 m	3430 vw		1125 sh	1124 m	ρ NH ₂ , ν CNC, ν CN ₃
3330 mb	3330 mb		1075 sh	1075 w	ν_3 HPO ₃ ^{2−}
	3225 mb		1050 s	1055 w	ν_2 HPO ₃ ^{2−} , ρ NH ₂ , ν CN ₃
3110 sb	3110 mb		1032 s	1035 m	ν_2 HPO ₃ ^{2−}
2940 sb		ν N–H(...N)	1021 s	1022 m	
2860 sb				1009 w	ν CN ₃ , ρ NH ₂
2745 sb			973 m	976 s	ν_3 HPO ₃ ^{2−}
2430 mb		?	900 m	905 s	δ CNC, ν CN, ρ NH ₂
2318 m	2329 m	ν_1 HPO ₃ ^{2−}	765 sh		π CN ₃ out of phase, γ CNH
	2279 vw	?		741 m	π CN ₃ in phase, γ CNH
2126 mb			725 s		
2033 w			655 sh	659 m	τ NH ₂ , δ CNC, δ CN ₃
1685 sh	1695 w	δ NH ₂ , ν CN ₃ , δ CN ₃ , ν CNC	600 s		ν_4 HPO ₃ ^{2−} , γ O–H(...O)
	1663 w	δ NH ₂ , ν CN ₃ , δ CN ₃ , δ CNC		575 m	ν_4 HPO ₃ ^{2−} , τ NH ₂ , γ CNC
1645 s	1646 w	δ NH ₂ , ν CN ₃ , δ CN ₃ , δ CNC, δ H ₂ O	444 m	452 s	ν_4 HPO ₃ ^{2−} , γ CNH, ω NH ₂
	1587 m	ν_{as} CNC, ν CN ₃ , δ CN ₃ , δ CNH		257 m	γ CNH, τ NH ₂
1560 s		ν_{s} CNC, ν CN ₃ , δ CN ₃ , δ CNH		237 m	δ CNC
1520 s	1529 w	δ CNC, ν CN ₃ , δ CN ₃ , δ NH ₂	195 m		External modes
1475 s	1481 w	ν CN ₃ , δ CN ₃ , δ NH ₂	158 m	159 vs	
1375 sh		?		130 s	External modes, γ CNC
1310 m			112 m		

Note. Abbreviations and symbols: vs, very strong; s, strong; m, medium; w, weak; vw, very weak; b, broad; sh, shoulder; ν , stretching; δ , deformation or in-plane bending; γ , π , out-of-plane bending; ρ , rocking; ω , wagging; τ , torsion; s, symmetric; as, antisymmetric.

Table 10
Correlation diagram of HPO_3^{2-} internal modes in **(bigua) $_2$ HPO $_3$ ·3H $_2$ O** and **biguaHPO $_3$ ·H $_2$ O** crystals

Free ion modes	Degrees of freedom	Free ion HPO_3^{2-} C_{3v}	Site symmetry C_1	Factor group C_1	Vibrational modes			
ν_1	2	A_1		$A_g(\text{Ra})$	$\nu_1, 2\nu_2, \nu'_3, 2\nu''_3, \nu'_4, 2\nu''_4$			
ν_2	2	E			$A_u(\text{IR})$	$\nu_1, 2\nu_2, \nu'_3, 2\nu''_3, \nu'_4, 2\nu''_4$		
ν'_3	2	A_1				$A_u(\text{IR})$	$\nu_1, 2\nu_2, \nu'_3, 2\nu''_3, \nu'_4, 2\nu''_4$	
ν''_3	2	E					$A_u(\text{IR})$	$\nu_1, 2\nu_2, \nu'_3, 2\nu''_3, \nu'_4, 2\nu''_4$
ν'_4	2	A_1						$A_u(\text{IR})$
ν	2	E	$A_u(\text{IR})$	$\nu_1, 2\nu_2, \nu'_3, 2\nu''_3, \nu'_4, 2\nu''_4$				

Table 12
Correlation diagram of NO_3^- internal modes for each of symmetry independent anion in **bigua(NO $_3$) $_2$**

Free ion modes	Degrees of freedom	Free ion NO_3^- D_{3h}	Site symmetry C_1	Factor group C_{2v}	Vibrational modes
ν_1	4	A'_1		$A_1(\text{IR, Ra})$	$\nu_1, \nu_2, 2\nu_3, 2\nu_4$
ν_2	4	A''_2		$A_2(\text{Ra})$	$\nu_1, \nu_2, 2\nu_3, 2\nu_4$
ν_3	4	E'		$B_1(\text{IR, Ra})$	$\nu_1, \nu_2, 2\nu_3, 2\nu_4$
ν_4	4	E'		$B_2(\text{IR, Ra})$	$\nu_1, \nu_2, 2\nu_3, 2\nu_4$

only in the IR spectrum at 837 and 735 cm^{-1} were assigned to the carbonate ν_2 and ν_4 vibrations, respectively.

The sharp, medium to strong band at 2344 cm^{-1} in the IR spectrum (2360 cm^{-1} Raman) of **biguaHPO $_3$ ·H $_2$ O** corresponds to the stretching P–H vibrations (ν_1 HPO_3^{2-}). Manifestations of the ν'_3 HPO_3^{2-} vibrations (overlapping with the ρ NH_2 , ν CN_3 vibrations) were found at 1086 and 1083 cm^{-1} in the IR and Raman spectra, respectively. The strong band at 1029 cm^{-1} in the IR spectrum (strong band at 1032 cm^{-1} and shoulder at 1024 cm^{-1} in the Raman spectrum) can be assigned to the P–H deformation vibrations (ν_2 HPO_3^{2-}). The intense bands at 971 cm^{-1} (IR) and 981 cm^{-1} (Raman) were assigned to the ν'_3 HPO_3^{2-} vibrations. Manifestations of the ν''_4 HPO_3^{2-} vibrations, which overlap with the δ CN_3 , γ CNH vibrations of the cation, were recorded at ca. 550 cm^{-1} in both the spectra. Finally, bands at 477 cm^{-1} (IR) and 482 cm^{-1} (Raman) were assigned to ν'_4 phosphite vibrations. The

observed level of factor group splitting of the anion vibrational bands is slightly lower than was expected (see Table 10).

Strong bands in the 1090–970 cm^{-1} region localized in the IR spectrum of **biguaHPO $_4$ ·H $_2$ O** can be assigned to manifestations derived from the originally triply degenerate phosphate ν_3 vibration (see Table 16) slightly overlapping with the ρ NH_2 , ν CN_3 vibrations. The band recorded at 952 cm^{-1} in the Raman spectrum (957 cm^{-1} IR spectrum) can be assigned to the ν_1 PO_4 vibration. The assignment of the almost symmetrical doublet found at 540 and 535 cm^{-1} in the IR spectrum (535 and 525 cm^{-1} Raman spectrum) can be derived from the degenerate phosphate ν_4 vibration mixed with the δ CN_3 , γ CNH modes. The bands present in both spectra in the 400–380 cm^{-1} region were assigned to the ν_2 PO_4 vibrations. Finally, bands recorded at approx. 1215 and 865 cm^{-1} were assigned to the manifestations of the δ POH and ν P–OH vibrations, respectively. The

Table 11
FTIR and FT Raman spectra of **bigua(NO $_3$) $_2$**

IR (cm^{-1})	Raman (cm^{-1})	Assignment	IR (cm^{-1})	Raman (cm^{-1})	Assignment
3330 mb	3310 wb	ν N–H(...O), ν N–H(...N)	1091 w		ρ NH_2 , ν CN_3
3145 mb	3230 wb		1077 m	1078 w	
2950 mb				1051 vs	ν_1 NO_3^-
2755 mb			1045 m	1044 vs	
2330 wb		?	950 w	950 m	δ CNC , ν CN , ρ NH_2
1760 w		$(\nu_1 + \nu_4)\text{NO}_3^-$	825 m		ν_2 NO_3^-
1704 s		δ NH_2 , δ NH , ν CN_3 , δ CN_3 , ν_{as} CNC	784 w		π CN_3 , γ CNH
1651 m	1650 w	δ NH_2 , ν CN_3 , δ CN_3	723 m	726 m	ν_4 NO_3^- , π CN_3 , γ CNH
	1634 w		713 m	713 m	
1618 m		δ CNC , ν CN_3 , δ CN_3	691 m		γ CNH , γ CNC , γ N–H(...O)
1579 w	1573 w	δ CNC , ν CN_3 , δ CN_3 , δ NH_2	675 m		
	1553 m	ν_{s} CNC , ν CN_3 , δ CN_3 , δ CNH	614 m	612 m	γ CNH , τ NH_2
1535 m	1537 w	ν CN_3 , δ CN_3 , δ NH_2	575 m		ω NH_2 , τ NH_2 , γ NH
1509 sh		?	538 m	557 w	δ CN_3 , γ CNH
1453 sh		ρ NH_2 , ν_{s} CNC , ν CN_3	444 w	447 m	ω NH_2 , γ CNH , γ NH
1418 s	1424 w		429 w	430 m	γ CNH , τ NH_2
1388 s	1380 w	ν_3 NO_3^-	248 w	245 w	
	1335 w		180 m		External modes
1317 s			120 m	158 s	
1169 m		ρ NH_2 , ν_{as} CNC , ν CN_3			
	1130 m	ρ NH_2 , ν_{s} CNC , ν CN_3			

Table 13
FTIR and FT Raman spectra of **biguaCO₃·H₂O**

IR (cm ⁻¹)	Raman (cm ⁻¹)	Assignment	IR (cm ⁻¹)	Raman (cm ⁻¹)	Assignment
3435 s		ν O–H(...O), ν N–H(...O), ν N–H(...N)	1053 m	1055 w	ρ NH ₂ , ν CN ₃
3380 s				1037 s	ν_1 CO ₃ ²⁻
3325 s	3340 w		1024 m		ν CN ₃ , ρ NH ₂
3190 s	3240 w			1008 w	
3119 sb	3115 w		914 m	915 s	δ CNC, ν CN, ρ NH ₂
2933 sb			875 m		γ N–H(...O)
2765 m			837 m		ν_2 CO ₃ ²⁻
2688 mb			795 m		γ O–H(...O), γ N–H(...O)
2440 mb			763 m	761 m	π CN ₃ , γ CNH
2270 sh		?	735 m		ν_4 CO ₃ ²⁻
2143 w			688 m		γ CNH, δ CNC
1688 s	1691 w	δ NH ₂ , δ NH, ν CN ₃ , δ CN ₃ , ν_{as} CNC	661 m		γ CNH, γ CNC
	1669 w		637 m	640 m	γ CNH, τ NH ₂
1657 s		δ NH ₂ , ν CN ₃ , δ CN ₃ , δ CNC, δ H ₂ O	582 m	579 m	ω NH ₂ , τ NH ₂ , γ NH
	1644 w		528 m		δ CN ₃ , γ CNH
1630 s	1631 w	δ NH ₂ , ν CN ₃ , δ CN ₃		468 m	ω NH ₂ , γ CNH, γ NH
	1548 w	ν_s CNC, ν CN ₃ , δ CN ₃ , δ CNH	451 m	452 s	γ CNH, τ NH ₂
1522 s	1527 w	ν CN ₃ , δ CN ₃ , δ NH ₂	271 w		γ CNH, τ NH ₂
1483 s	1498 sh	ρ NH ₂ , ν_s CNC, ν CN ₃		251 m	
1401 s	1400 w	ν_3 CO ₃ ²⁻	226 sh		External modes
1348 s			182 m	176 m	
	1304 w	?	153 m	145 vs	
1223 m			130 m	135 vs	
1153 m		ρ NH ₂ , ν_{as} CNC, ν CN ₃	106 m		
1106 m	1120 m	ρ NH ₂ , ν_s CNC, ν CN ₃			

Table 14
FTIR and FT Raman spectra of **biguaHPO₃·H₂O**

IR (cm ⁻¹)	Raman (cm ⁻¹)	Assignment	IR (cm ⁻¹)	Raman (cm ⁻¹)	Assignment
	3200 mb	ν O–H(...O), ν N–H(...O)		1024 sh	ν_2 HPO ₃ ²⁻
3140 sb				1010 sh	ν CN ₃ , ρ NH ₂
2945 sb		ν N–H(...O), ν N–H(...N)	971 s	981 s	ν_3' HPO ₃ ²⁻
2780 sb		ν N–H(...O)	925 m	944 s	δ CNC, ν CN, ρ NH ₂
2344 s	2360 m	ν_2 HPO ₃ ²⁻	865 m		γ N–H(...O)
2328 sh			765 m		π CN ₃ , γ CNH
1730 sh		δ NH ₂ , ν CN ₃ , δ CN ₃ , δ CNC	723 m	735 w	
1695 s	1685 w	δ NH ₂ , δ NH, ν CN ₃ , δ CN ₃ , ν_{as} CNC	700 m		ω NH ₂ , γ NH, γ CNH, γ N–H(...O)
1641 s		δ NH ₂ , ν CN ₃ , δ CN ₃ , δ CNC, δ H ₂ O	642 m	637 w	γ CNH, τ NH ₂ , γ O–H(...O)
	1600 w	δ NH ₂ , ν CN ₃ , δ CN ₃	590 m	598 m	ω NH ₂ , τ NH ₂ , γ NH
1545 sh	1541 m	ν_s CNC, ν CN ₃ , δ CN ₃ , δ CNH	551 m	548 w	ν_4'' HPO ₃ ²⁻ , δ CN ₃ , γ CNH
1524 s		ν CN ₃ , δ CN ₃ , δ NH ₂	477 m	482 s	ν_4' HPO ₃ ²⁻
1449 s	1455 w	ρ NH ₂ , ν_s CNC, ν CN ₃	452 m	449 vs	γ CNH, τ NH ₂
1353 m		?		271 w	
1197 w			204 m		δ C–N–C
1152 w	1155 s	ρ NH ₂ , ν_{as} CNC, ν CN ₃	162 m	162 vs	External modes
1086 s	1083 m	ν_3'' HPO ₃ ²⁻ , ρ NH ₂ , ν CN ₃		149 s	
1029 s	1032 s	ν_2 HPO ₃ ²⁻		124 s	

observed factor group splitting is very close to the results of correlation analysis presented in Table 16.

3.4. Second harmonic generation

Only crystals of **bigua(NO₃)₂** fulfil the symmetry condition (space group *P* ca2₁) for second harmonic generation within the group of studied biguanidinium salts with resolved crystal structures. Subsequent measurements of the SHG efficiency for powdered **bigua(NO₃)₂** and **biguaCO₃·H₂O**

were performed at 800 nm. The relative SHG efficiency was observed as equal to 87% (**bigua(NO₃)₂**) and 20% (**biguaCO₃·H₂O**) compared to KDP.

4. Conclusions

Five inorganic salts of biguanide were prepared and studied in this paper. X-ray structural analysis has been performed for three novel salts with phosphoric and phosphorous acids. The crystal structure of (**bigua**)₂H-

Table 15
FTIR and FT Raman spectra of **biguaHPO₄·H₂O**

IR (cm ⁻¹)	Raman (cm ⁻¹)	Assignment	IR (cm ⁻¹)	Raman (cm ⁻¹)	Assignment
3568 w		ν O–H(...O), ν N–H(...O)		952 m	ν_1 PO ₄
3455 sh	3465 w		910 m	914 s	δ CNC, ν CN, ρ NH ₂
3424 s			864 s	860 sh	ν P–OH, γ N–H(...O)
3340 s	3360 wb		768 m	759 m	π CN ₃ , γ CNH, γ O–H(...O)
	3315 wb		727 m		
	3225 wb		648 m	646 m	γ CNH, δ CNC
3050 sb		ν O–H(...O), ν N–H(...O), ν N–H(...N)		584 m	γ CNH, ω NH ₂
2770 sb		ν N–H(...O)		574 m	ω NH ₂ , τ NH ₂ , γ NH
2430 sh			540 m	535 m	ν_4 PO ₄ , δ CN ₃ , γ CNH
2140 sh		?	525 m	525 sh	
1666 s	1655 w	δ NH ₂ , ν CN ₃ , δ CN ₃ , δ CNC		477 sh	τ NH ₂ , γ CNC
1639 s		δ NH ₂ , ν CN ₃ , δ CN ₃	462 m	461 s	ω NH ₂ , γ CNH, γ NH
1550 s	1541 m	ν_s CNC, ν CN ₃ , δ CN ₃ , δ CNH		444 sh	γ CNH, τ NH ₂
1464 s	1475 sh	ρ NH ₂ , ν_s CNC, ν CN ₃	400 m	400 m	ν_2 PO ₄
1213 m	1220 vw	δ POH	383 sh	383 m	
	1112 m	ρ NH ₂ , ν_s CNC, ν CN ₃	335 sh		?
1086 s	1088 sh	ν_3 PO ₄ , ρ NH ₂ , ν CN ₃	272 w	251 m	γ CNH, τ NH ₂
1046 s	1053 w		170 m		External modes
	1009 w	ν CN ₃ , ρ NH ₂		150s	
982 s	977 w	ν_3 PO ₄	126 m		
957 s			98 w		

Table 16
Correlation diagram of HPO₄²⁻ internal modes in **biguaHPO₄·H₂O** crystal

Free ion modes	Degrees of freedom	Free ion PO ₄ ³⁻ T _d	Free ion HPO ₄ ²⁻ C _{3v}	Site symmetry C ₁	Factor group C ₁	Vibrational modes
ν_1	2	A ₁	A ₁	A ₁	A _g (Ra)	$\nu_1, 2\nu_2, 3\nu_3, 3\nu_4$
ν_2	2	E	E	E		
ν_3	2	F ₂	E	A ₁		
			E	E		
ν_4	2	F ₂	E	A ₁	A _u (IR)	$\nu_1, 2\nu_2, 3\nu_3, 3\nu_4$
			E	E		

PO₃·3H₂O is based on a network of phosphite anions and water molecules. This network is filled by biguanidium(1+) cations, which form pairs through two intermolecular hydrogen bonds of the N–H...N type. The crystal structure of **biguaHPO₃·H₂O** is formed of a network of alternating biguanidium(2+) cations, phosphite anions and pairs of water molecules interconnected by a system of intermolecular hydrogen bonds. Finally, the **biguaHPO₄·H₂O** crystal structure is formed by pairs of anions that are mutually joined in chains through two water molecules. These chains are interconnected by biguanidium(2+) cations (via N–H...O hydrogen bonds) to form a three-dimensional network.

The FTIR and FT Raman spectra of all five compounds were recorded and their interpretation is based on quantum-chemical calculations of the vibrational modes of the biguanidium(1+) and biguanidium(2+) cations.

The results of SHG measurements indicate that **biguaCO₃·H₂O** (SHG efficiency 20% of KDP) crystallises in a non-centrosymmetric space group. Both studied salts, i.e. **biguaCO₃·H₂O** and **bigua(NO₃)₂**, exhibit optical transpar-

ency down to 255 nm and are stable up to their melting points at 374 and 453 K, respectively. These properties, together with the higher SHG efficiency of **bigua(NO₃)₂** (87% of KDP), lead to the conclusion that especially this salt can be considered to be a promising novel NLO material.

Acknowledgements

This work was financially supported by the Grant Agency of Charles University in Prague (Grant No. 337/2005/B-Ch) and is part of the long term Research Plan of the Ministry of Education of the Czech Republic No. MSM0021620857.

References

- [1] A. Marchi, L. Marvelli, M. Cattabriga, R. Rossi, M. Neves, V. Bertolasi, V. Ferretti, J. Chem. Soc., Dalton Trans. (1999) 1937.
- [2] P. Ray, Chem. Rev. 61 (1961) 313.
- [3] C.R. Sirtori, C. Pasik, Pharmacol. Res. 30 (1994) 187.
- [4] B. Clement, U. Girreser, Magn. Reson. Chem. 37 (1999) 662.
- [5] K.H. Thompson, J.H. McNeill, C. Orvig, Chem. Rev. 99 (1999) 2561.
- [6] S.A. Ross, E.A. Gulve, M. Wang, Chem. Rev. 104 (2004) 1255.
- [7] L.C.Y. Woo, V.G. Yuen, K.H. Thompson, J.H. McNeill, C. Orvig, J. Inorg. Biochem. 76 (1999) 251.
- [8] W.M. Watkins, J.D. Chulay, D.G. Sixsmith, H.C. Spencer, R.E. Howells, J. Pharm. Pharmacol. 39 (1987) 261.
- [9] P. Morain, C. Abraham, B. Portevin, G. De Nanteuil, Mol. Pharmacol. 46 (1994) 732.
- [10] S.L. Shapiro, V.A. Parrino, E. Rogow, L. Freedman, J. Am. Chem. Soc. 81 (1959) 3725.
- [11] S.L. Shapiro, V.A. Parrino, L. Freedman, J. Am. Chem. Soc. 81 (1959) 2220.
- [12] K.B. Anderson, R.A. Franich, H.W. Kroese, R. Meder, Polyhedron 14 (1995) 1149.
- [13] N.B. Bolotina, M.J. Hardie, A.A. Pinkerton, J. Appl. Cryst. 36 (2003) 1334.

- [14] A. Martin, A.A. Pinkerton, R.D. Gilardi, J.C. Bottaro, *Acta Crystallogr. B: Struct. Sci.* 53 (1997) 504.
- [15] E.A. Zhurova, A. Martin, A.A. Pinkerton, *J. Am. Chem. Soc.* 124 (2002) 8741.
- [16] J. Zyss, J. Pecaut, J.P. Levy, R. Masse, *Acta Crystallogr. B* 49 (1993) 334.
- [17] C.B. Aakeröy, P.B. Hitchcock, B.D. Moyle, K.R. Seddon, *J. Chem. Soc. Chem. Commun.* 23 (1989) 1856.
- [18] C.B. Aakeröy, K.R. Seddon, *Chem. Soc. Rev.* 22 (6) (1993) 397.
- [19] D. Xue, S. Zhang, *J. Phys. Chem. Solids* 57 (1996) 1321.
- [20] D. Xue, S. Zhang, *J. Phys. Chem. A* 101 (1997) 5547.
- [21] A. Martin, A.A. Pinkerton, A. Schiemann, *Acta Cryst. C* 52 (1996) 966.
- [22] A. Martin, A.A. Pinkerton, *Acta Cryst. C* 52 (1996) 1048.
- [23] A.A. Pinkerton, D. Schwarzenbach, *J. Chem. Soc. Dalton* (1978) 989.
- [24] S.R. Ernst, *Acta Crystallogr. B: Struct. Crystallogr. Cryst. Chem.* B33 (1977) 237.
- [25] J.M. Adams, R.G. Pritchard, *J. Appl. Cryst.* 8 (1975) 392.
- [26] H. Ratajczak, J. Baran, J. Barycki, S. Debrus, M. May, A. Pietraszko, H.M. Ratajczak, A. Tramer, J. Venturini, *J. Mol. Struct.* 555 (2000) 149.
- [27] T. Glowiak, S. Debrus, M. May, A.J. Barnes, H. Ratajczak, *J. Mol. Struct.* 596 (2001) 77.
- [28] D.P. Shelton, J.E. Rice, *Chem. Rev.* 94 (1994) 3.
- [29] C. Castiglioni, M. Del-Zoppo, G. Zerbi, *Phys. Rev. B* 53 (1996) 13319.
- [30] D.M. Bishop, B. Kirtman, *Rev. B* 56 (1997) 2273.
- [31] C. Castiglioni, M. Del-Zoppo, G. Zerbi, *Phys. Rev. B* 56 (1997) 2275.
- [32] D.M. Bishop, B. Champagne, B. Kirtman, *J. Chem. Phys.* 109 (1998) 9987.
- [33] S.H.M. Söntjens, J.T. Meijer, H. Kooijman, A.L. Spek, M.H.P. van Genderen, R.P. Sijbesma, E.W. Meijer, *Org. Lett.* 24 (3) (2001) 3887.
- [34] A. Altomare, M.C. Burla, M. Camalli, G. Cascarano, C. Giacovazzo, A. Guagliardi, G. Polidori, SIR97 – *J. Appl. Crystallogr.* 27 (1994) 435.
- [35] G.M. Sheldrick, SHELXL 97, Program for Refinement from Diffraction Data, University of Göttingen Germany, Göttingen, 1997.
- [36] Gaussian 98, Revision A.11, M.J. Frisch, G.W. Trucks, H.B. Schlegel, G.E. Scuseria, M.A. Robb, J.R. Cheeseman, V.G. Zakrzewski, J.A. Montgomery, Jr., R.E. Stratmann, J.C. Burant, S. Dapprich, J.M. Millam, A.D. Daniels, K.N. Kudin, M.C. Strain, O. Farkas, J. Tomasi, V. Barone, M. Cossi, R. Cammi, B. Mennucci, C. Pomelli, C. Adamo, S. Clifford, J. Ochterski, G.A. Petersson, P.Y. Ayala, Q. Cui, K. Morokuma, P. Salvador, J.J. Dannenberg, D.K. Malick, A.D. Rabuck, K. Raghavachari, J.B. Foresman, J. Cioslowski, J.V. Ortiz, A.G. Baboul, B.B. Stefanov, G. Liu, A. Liashenko, P. Piskorz, I. Komaromi, R. Gomperts, R.L. Martin, D.J. Fox, T. Keith, M.A. Al-Laham, C.Y. Peng, A. Nanayakkara, M. Challacombe, P.M.W. Gill, B. Johnson, W. Chen, M.W. Wong, J.L. Andres, C. Gonzalez, M. Head-Gordon, E.S. Replogle, and J.A. Pople, Gaussian, Inc., Pittsburgh PA, 2001.
- [37] GaussViewW, version 2.1, Gaussian, Inc., Pittsburgh, PA, 2001.
- [38] NIST Computational Chemistry Comparison and Benchmark Database, NIST Standard Reference Database Number 101 Release 10, May 2004, Editor: Russell D. Johnson III, <http://srdata.nist.gov/cccbdb/vibscalejust.asp>.
- [39] A.L. Spek, *J. Appl. Cryst.* 36 (2003) 7.
- [40] M. Tsuboi, *J. Am. Chem. Soc.* (1957) 1351.
- [41] J. Baran, M.M. Ilczyszyn, M. Sledz, H. Ratajczak, *J. Mol. Struct.* 526 (2000) 235.
- [42] A. Ghule, Ch. Bhongale, H. Chang, *Spectrochim. Acta A* 59 (2003) 1529.
- [43] A. Hadrich, A. Lautié, T. Mhiri, F. Romain, *Vib. Spectrosc.* 26 (2001) 51.
- [44] A. Lautié, F. Froment, A. Novak, *Spectrosc. Lett.* 9 (1976) 289.
- [45] A. Novak, *Struct. Bonding* 18 (1973) 177.